



# Influences of harmonic cavities on single-bunch instabilities in electron storage rings

Hai-Sheng Xu<sup>1</sup> · Jing-Ye Xu<sup>1,2</sup> · Na Wang<sup>1</sup>

Received: 20 April 2021 / Revised: 4 August 2021 / Accepted: 5 August 2021 / Published online: 30 August 2021

© China Science Publishing & Media Ltd. (Science Press), Shanghai Institute of Applied Physics, the Chinese Academy of Sciences, Chinese Nuclear Society 2021

**Abstract** Harmonic cavities (HCs) are widely used in electron storage rings, mainly to increase the Touschek lifetime by lengthening bunches. HCs have become critical components of almost all fourth-generation synchrotron light sources. In addition to the benefits of increasing the Touschek lifetime, they also affect the collective beam instabilities in electron storage rings. However, the influence of HC settings on collective beam instabilities is still not well understood. HCs are typically designed to operate under so-called ideal lengthening conditions, which do not necessarily optimize the suppression of collective beam instabilities. We therefore extended earlier studies of collective beam instabilities to consider more general HC settings. We present preliminary studies and analyses of the influences of different HC settings on microwave and transverse mode-coupling instabilities.

**Keywords** Harmonic cavity · Microwave instability · Transverse Mode-coupling instability

---

This work was supported by the National Natural Science Foundation of China (Nos. 11805217 and 11775239), the Youth Innovation Promotion Association CAS, and NKPSTRD (No. 2016YFA0402001).

---

✉ Hai-Sheng Xu  
xuhs@ihep.ac.cn  
Na Wang  
wangn@ihep.ac.cn

<sup>1</sup> Key Laboratory of Particle Acceleration Physics and Technology, Institute of High Energy Physics, Chinese Academy of Sciences, Beijing 100049, China

<sup>2</sup> University of the Chinese Academy of Sciences, Beijing 100049, China

## 1 Introduction

Harmonic cavities (HCs) are widely studied and used in the electron storage rings of many existing synchrotron light sources. Their main purpose is to improve the beam lifetime, in particular the Touschek lifetime [1–6]. The typical so-called ideal setting of an HC is that which satisfies the ideal lengthening (or optimal lengthening) condition, namely that the RF potential around the synchronous phase is flat. Such an ‘ideal HC’ increases the bunch length significantly.

The successful application of HCs has led to their wider usage in fourth-generation synchrotron light sources based on diffraction-limited storage rings (DLSRs) [7–12]. However, implementing HCs causes side effects alongside bunch lengthening, such as variations in the longitudinal potential well, changes in the synchrotron oscillation frequency, and differences in the synchrotron oscillation frequency spread. Under the ‘ideal HC’ setting, the synchrotron oscillation frequency of the particles in a bunch decreases remarkably, while the synchrotron oscillation frequency spread of the particles in each bunch increases significantly. Both effects dramatically increase the complexity of instabilities in an electron storage ring. The overall influence of HCs on the beam dynamics, especially on the collective beam instabilities, is therefore paramount and merits further investigation.

Many studies have been conducted on collective beam instabilities while considering HCs, predominantly under ‘ideal-lengthening’ conditions. However, many other more general HC settings exist that produce ‘non-ideal lengthening’. The lack of systematic comparisons between ideal and non-ideal lengthening conditions has motivated us to study the influences of different HC settings on the

thresholds or growth rates of collective beam instabilities in electron storage rings [13]. Because single-bunch instabilities strongly limit the single-bunch charge and the corresponding beam quality, we first examined two important single-bunch instabilities found in electron storage rings: microwave instability (MWI) and transverse mode-coupling instability (TMCI).

Because of the much smaller vacuum chambers in DLSRs, the resistive wall (RW) impedance is considered to contribute significantly (even predominantly) to the total broadband impedance (especially in the transverse direction) [7, 14, 15]. Therefore, we used only the RW impedance in the present study.

The toy lattice used here was a previous storage ring lattice of the High Energy Photon Source (HEPS) [10]. The relevant parameters are listed in Table 1. The RW impedance is obtained assuming a round vacuum chamber (radius of 10 mm) made of stainless steel along the entire ring.

This study presents a preliminary investigation of the MWI and TMCI thresholds under the conditions defined by different HC settings, assuming active HCs. The paper is organized as follows. Section 2 briefly reviews the basic longitudinal dynamics of a double-RF system as well as the ideal lengthening condition. Then, MWI and TMCI thresholds without an HC and with an ‘ideal HC’ are investigated in Sect. 3. These studies are extended to cover general HC settings. Several classic settings corresponding to ‘non-ideal lengthening’ conditions are presented in Sect. 4. MWI and TMCI thresholds under different HC settings are compared in Sect. 5. Section 6 concludes with a discussion.

**Table 1** Main parameters of the toy lattice

Parameter	Value
Circumference, $C$ (m)	1360.4
Beam energy, $E_0$ (GeV)	6
Total current, $I_0$ (mA)	200
Betatron tune ( $x,y$ ), $\nu_{x,y}$	114.14/106.23
Momentum compaction factor, $\alpha_c$	$1.56 \times 10^{-5}$
Natural energy spread, $\delta_p/p$	$1.06 \times 10^{-3}$
Average energy loss per turn, $U_0$ (MeV)	2.89
Harmonic number of primary RF, $h_1$	756
Frequency of the primary RF, $f_0$ (MHz)	166.60
Harmonic number ratio of HC, $h_2/h_1$	3
Frequency of the HC, $f_{HC}$ (MHz)	499.80

## 2 Brief overview of the theory in a double RF system

The wide use of double-RF systems has motivated the development of the basic theory of longitudinal beam dynamics in that context. This section provides a brief textbook review of HC theory (see, e.g., [16]).

Following the form of the equations for longitudinal motion with only one RF system, similar equations can be written, considering both a primary RF system and an HC:

$$\begin{aligned} \dot{\delta} &= \frac{e\omega_0}{2\pi\beta^2 E} [V_1(\sin \phi_1 - \sin \phi_{1s}) + V_2(\sin \phi_2 - \sin \phi_{2s})], \\ \dot{\phi}_1 &= h_1\omega_0\eta\delta, \end{aligned} \tag{1}$$

where  $\delta$  is the relative momentum deviation of a particle,  $\omega_0$  is the angular revolution frequency,  $E$  is the particle energy, and  $\eta$  is the phase slip factor. The subscripts 1 and 2 denote the primary RF system and the HC, respectively. (For instance,  $V_1$  and  $V_2$  represent the peak voltages of the primary RF and the HC, respectively.  $\phi_{1s}$  and  $\phi_{2s}$  are the synchronous phases of the primary RF and the HC, respectively.) Because the HC resonant frequency is an integer harmonic of the primary RF, the relationship between phases  $\phi_1$  and  $\phi_2$  can be expressed as  $\phi_2 = \phi_{2s} + h(\phi_1 - \phi_{1s})$ , where  $h = h_2/h_1$  is the ratio between the harmonic numbers of the HC ( $h_2$ ) and primary RF ( $h_1$ ). Therefore, the Hamiltonian can be expressed as:

$$\begin{aligned} H &= \frac{1}{2}h_1\omega_0\eta\delta^2 + \frac{e\omega_0}{2\pi\beta^2 E} \{V_1[(\cos \phi_1 - \cos \phi_{1s}) \\ &+ (\phi_1 - \phi_{1s}) \sin \phi_{1s}] + \frac{V_2}{h} [\cos(\phi_{2s} + h(\phi_1 - \phi_{1s})), \\ &- \cos \phi_{2s} + h(\phi_1 - \phi_{1s}) \sin \phi_{2s}]\}. \end{aligned} \tag{2}$$

This Hamiltonian describes the longitudinal motions of particles under any HC setting, including the widely used ‘ideal HC’ setting. In the following, we briefly review the ‘ideal lengthening’ condition.

The total RF voltage  $V_{\text{total}}$ , provided by the double RF system, can be expressed in terms of the peak voltages and phases of the primary RF and HC as

$$V_{\text{total}} = V_1 \sin \phi_1 + V_2 \sin \phi_2, \tag{3}$$

where the peak voltages and synchronous phases of the primary cavity and the HC should be set to compensate for the average radiation energy loss per turn  $U_0$ :

$$U_0 = eV_1 \sin \phi_{1s} + eV_2 \sin \phi_{2s}. \tag{4}$$

As mentioned above, the ‘ideal lengthening’ condition corresponds to the RF potential being stationary around the

synchronous phase of the primary cavity. It is determined by setting both the first and second derivatives of the total RF voltage in the synchronous phase to zero:

$$\begin{aligned} \frac{\partial V_{\text{total}}}{\partial \phi_1} \Big|_{\phi_1=\phi_{1s}} &= 0, \\ \frac{\partial^2 V_{\text{total}}}{\partial \phi_1^2} \Big|_{\phi_1=\phi_{1s}} &= 0. \end{aligned} \tag{5}$$

Using Eq. (5), the values  $V_1, \phi_{1s}, V_2, \phi_{2s}$  can be calculated for an arbitrary RF bucket height. For example, Fig. 1 shows the normalized bunch distribution in the longitudinal direction under the conditions without HC and with ‘ideal HC’. Two methods are used in the calculations: analytic computation and multiparticle tracking. Multiparticle tracking was performed using the elegant code [17] and its parallel version Pelegant [18]. A total of one million macroparticles were tracked for 50,000 turns (corresponding to approximately 14 times the longitudinal radiation damping time and 12 times the vertical damping time) to ensure convergence to the equilibrium state.

Excellent agreement is achieved, as shown in Fig. 1. Furthermore, Fig. 1 also shows that the root-mean-square (RMS) bunch length increased from approximately 16.15 ps to approximately 97.04 ps when implementing the ‘ideal HC’ conditions. The approximate six-fold bunch lengthening caused a significant reduction in the peak bunch intensity.

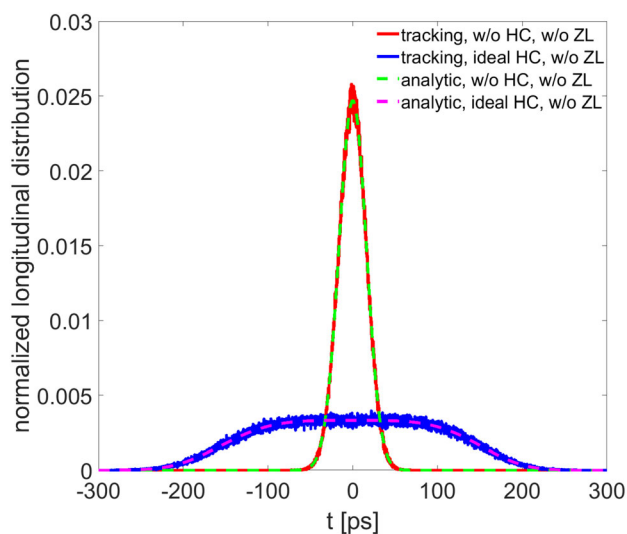


**Fig. 1** (Color online) Equilibrium longitudinal distributions under the conditions without HC and with ‘ideal HC’, neglecting any collective effects. The red solid curve and the green dashed curve represent the equilibrium distributions without considering HC, obtained by the multi-particle tracking and analytic method, respectively. The blue solid curve and the magenta dashed curve represent the equilibrium distributions with ‘ideal HC’, as obtained using multiparticle tracking and the analytic method, respectively

### 3 MWI and TMCI without HC and with ideal HC

Before exploring the MWI and TMCI thresholds under more general HC settings, we studied these two single-bunch instabilities under conditions without HC and with an ideal HC.

The Boussard-Keil-Schnell criterion [19] is a convenient analytic method for estimating the MWI threshold without considering any HC. However, it is widely accepted that the Boussard-Keil-Schnell criterion usually gives significantly lower threshold current. For situations with an ideal HC, the analytic method for estimating MWI is still under development. Therefore, the MWI threshold is usually determined via multiparticle tracking in the presence of HCs. Figure 2 shows the tracking results of the bunch energy spread corresponding to different single-bunch charges, indicating that the implementation of an ideal HC results in higher MWI threshold current. The tracking simulations were performed using the elegant code, using 1 million macroparticles, tracked for 50,000 turns, as described above. The so-called final energy spread was computed by averaging the turn-by-turn energy spread of the last 10,000 turns (approximately the last 3 longitudinal damping times). The error bars represent standard deviations. To allow a fair comparison, we define the MWI threshold charge as the single-bunch charge value corresponding to 1% growth of the natural energy spread without considering longitudinal impedance.

The normalized bunch distributions corresponding to different single-bunch charges (Fig. 3) show that the potential well distortion (PWD) drives more electrons toward the head of the bunch as the single-bunch charge increases. The resulting higher local charge density at the

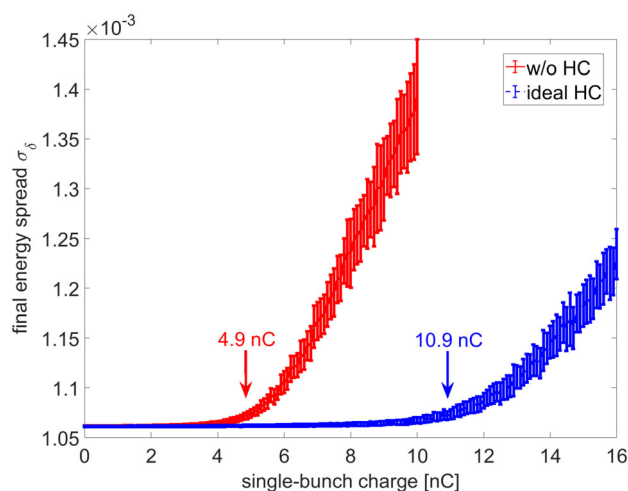


**Fig. 2** (Color online) ‘Final’ energy spread corresponding to different single-bunch charges. The red and blue curves represent the results obtained under conditions without an HC and with an ideal HC, respectively

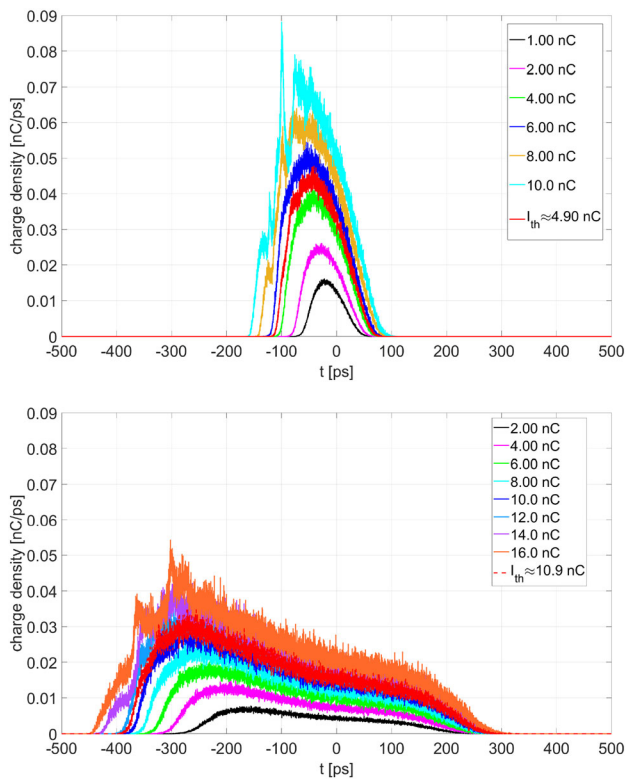


**Fig. 3** (Color online) Longitudinal distributions corresponding to different single-bunch charges either (upper plot) without an HC or (lower plot) with an ideal HC

bunch head causes the instability to originate from the bunch head. This motivates the conclusion that the MWI threshold current could be increased by moving more particles to the bunch tail, for example, by creating a specific RF potential. This was also a motivation for studying the ‘non-ideal HC’ settings.

HCs also affect the TMCI threshold. We studied the TMCI first without considering HCs. By setting the chromaticity to zero and including the vertical RW impedance, the TMCI threshold was obtained both theoretically and by simulation, giving very good agreement (Fig. 4).

We also performed multiparticle tracking keeping all other conditions the same, except from including an ideal HC. A higher TMCI threshold was obtained under the ‘ideal HC’ condition, as shown in Fig 5.

#### 4 Typical HC settings with non-ideal lengthening

The previous section systematically compared the effects of the longitudinal and transverse impedances on MWI and TMCI, respectively. Two typical conditions (namely, without HC and with ‘ideal HC’) were used. However, as argued above, much can be learned by considering more general ‘non-ideal lengthening’ conditions,

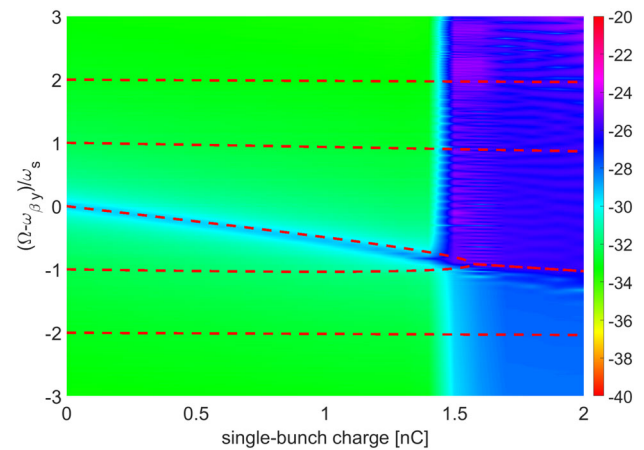


**Fig. 4** (Color online) Vertical modes vs. single-bunch charge obtained theoretically (red dashed lines) and using elegant tracking, considering only a vertical impedance

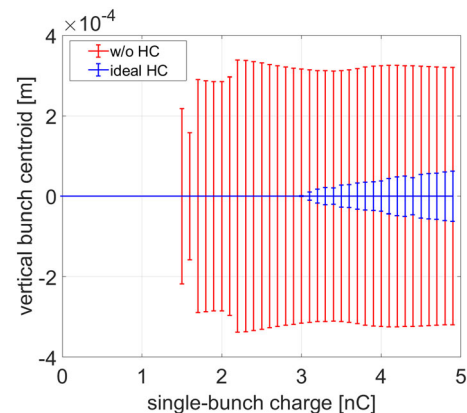


**Fig. 5** (Color online) Vertical positions of the bunch centroid vs. the single-bunch charge. The red and blue curves indicate the results obtained without considering HC and with ‘ideal HC’, respectively

as these are more common in the daily operations of many existing storage rings with HCs. ‘Non-ideal lengthening’ conditions can generally be classified as follows:

- sub-ideal lengthening with more particles at the bunch head. This indicates that the HC is set to make the bunch significantly longer than the situation without an HC, slightly shorter than the bunch length with an ‘ideal HC’, and with more particles at the head of the bunch (sets #1 - #5);
- sub-ideal lengthening with more particles at the bunch tail. This indicates that the HC is set to make the bunch significantly longer than the situation without an HC, slightly shorter than the bunch length with an ‘ideal HC’, and with more particles at the tail of the bunch (sets #6 - #10);
- overstretching (‘double-hump’ distribution). This indicates that the HC is set to make the bunch longer than the situation with an ‘ideal HC’ (sets #11 - #15).

The RF voltages and phases of the different settings mentioned above, together with the equilibrium bunch lengths (without considering any collective effect) are listed in Table 2. The values listed under ‘ideal HC’ are also given in Table 2 for comparison. The corresponding equilibrium distributions are shown in Fig. 6 and are grouped according to three typical situations.

### 5 MWI and TMCI under ‘non-ideal lengthening’ conditions

This section presents and analyzes the simulation results corresponding to the 15 typical ‘non-ideal HC’ settings described above, which can be classified into the above three groups.

The ‘final’ energy spread and the ‘net’ growth rates corresponding to the 15 typical HC settings are shown in Figs. 7 and 8. We obtained Fig. 7 by using the turn-by-turn energy spread data from 40,001 to 50,000 turns (approximately the last three damping times) at each bunch charge to calculate the average values and standard deviations (presented as mean values and error bars). The blue curves were obtained using an ‘ideal HC’. To obtain the ‘net’ growth rates shown in Fig. 8, the oscillation of the bunch centroid was used to fit an exponential function for the growth rates. Synchrotron radiation damping and quantum

excitation are included in the tracking. When the fitted ‘net’ growth rate approached zero, the bunch intensity was below the TMCI threshold current.

The thresholds for MWI (red cross markers) and TMCI (red pentagram markers) corresponding to all the above HC settings are shown in Fig. 9. The RMS bunch lengths, obtained without considering any collective effect, are represented in Fig. 9 with the blue ‘+’ markers. The red lines indicate the the threshold charges corresponding to the ideal HC settings, while the blue dashed lines are the RMS bunch length when using an ‘ideal HC’.

Unsurprisingly, the left plot of Fig. 9 shows the threshold charges of the HC settings for sets #1 - #5 being all lower than those of the ‘ideal HC’ situation. In addition, the threshold charges of sets #11 - #15 are all higher than those of the ‘ideal HC’ situation. Intuitively, a longer bunch should have a lower density. More interestingly in sets #6 - #10 (corresponding to situations with more particles at the bunch tails), the MWI threshold charges are sometimes higher than the ideal HC situation, despite the bunches being always shorter than in the ‘ideal HC’ situation. Therefore, this indicates that a higher MWI threshold charge might be obtained by putting more electrons in the bunch tail.

A more interesting phenomenon is apparent in the right plot of Fig. 9. Under both HC settings (sets #1 - #5 and #11 - #15), some situations display higher TMCI threshold charges than the ‘ideal HC’ situation. This cannot be fully explained using longer or shorter bunches. When putting more electrons in the bunch tail (sets #6 - #10), the TMCI threshold charges are all surprisingly significantly higher than in the ‘ideal HC’ situation.

**Table 2** Main RF settings (voltages and phases) and corresponding bunch lengths, obtained without considering the impedance

Index	$V_1$ (MV)	$\phi_{s1}$	$V_{HC}$ (MV)	$\phi_{sHC}$	$\sigma_{r0}$ (ps)
Ideal HC	3.6395	2.0390	0.6558	5.7005	97.04
Set #1	3.6395	1.9203	0.6590	5.3423	93.90
Set #2	3.6395	1.9028	0.6610	5.2898	90.20
Set #3	3.6395	1.8928	0.6623	5.2598	86.72
Set #4	3.6395	1.8714	0.6656	5.1956	76.05
Set #5	3.6395	1.8536	0.6689	5.1420	65.35
Set #6	3.6395	2.1466	0.6558	6.0276	94.36
Set #7	3.6395	2.1534	0.6558	6.0490	92.65
Set #8	3.6395	2.1576	0.6558	6.0621	91.33
Set #9	3.6395	2.1349	0.6531	5.9901	89.82
Set #10	3.6395	2.1669	0.6558	6.0914	87.52
Set #11	3.6504	2.0331	0.7017	-0.5743	225.27
Set #12	3.6759	2.0391	0.7017	-0.5950	157.00
Set #13	3.6450	2.0370	0.6754	-0.5782	142.36
Set #14	3.6504	2.0427	0.6754	-0.5700	130.78
Set #15	3.6439	2.0384	0.6689	-0.5786	123.27

### 6 Conclusions and discussions

Harmonic cavities have been widely used in storage rings, especially in fourth-generation DLSR-based synchrotron light sources. HCs can increase the Touschek lifetime, but are also used to stabilize the beams. Instability studies typically use HCs to achieve ‘ideal lengthening’.

We investigated MWI and TMCI, the two most important single-bunch instabilities encountered in storage rings, under conditions without HC and with an ‘ideal HC’. Higher threshold currents were achieved for both MWI and TMCI when implementing an ‘ideal HC’. To explore beyond ‘ideal lengthening’ conditions, we studied MWI and TMCI under more general HC settings.

‘Non-ideal lengthening’ conditions were classified into three groups: sub-ideal lengthening with more particles at the bunch head, sub-ideal lengthening with more particles at the bunch tail, and overstretching. To provide sufficient generality, we studied five different HC settings in each

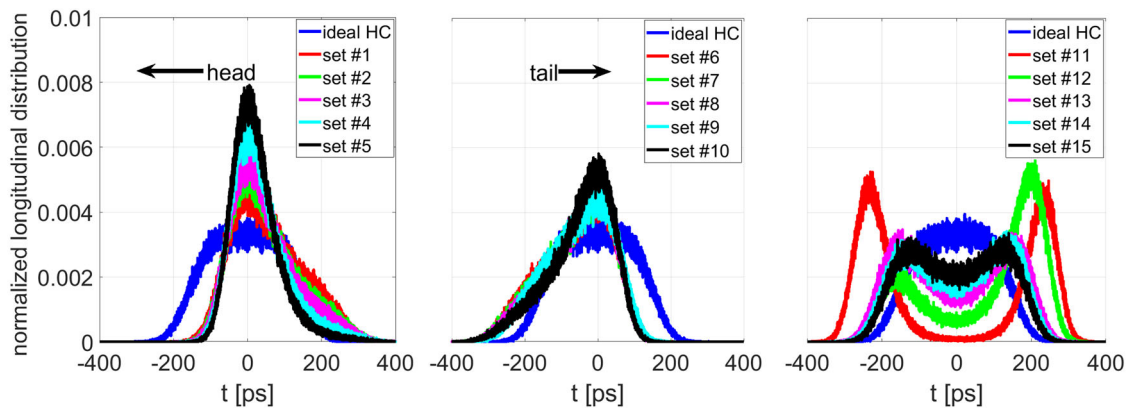


**Fig. 6** (Color online) Bunch distributions under HC settings with ‘non-ideal lengthening’, as given in Table 2. The blue curves represent the bunch distributions with an ‘ideal HC’, which served as the reference. Three groups of typical HC settings are represented

(left: sub-ideal lengthening with more particles at the bunch head; middle: sub-ideal lengthening with more particles at the bunch tail; and right: over-stretching)

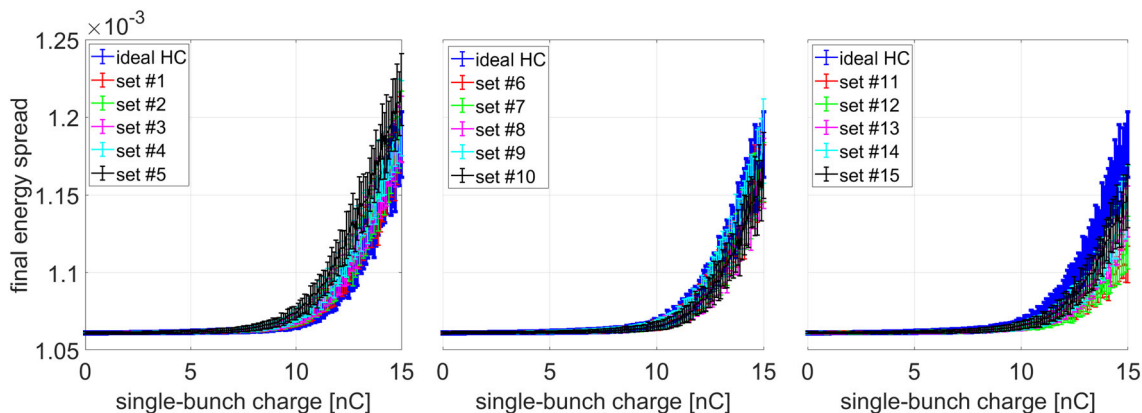


**Fig. 7** (Color online) ‘Final’ energy spread for different single-bunch charges, corresponding to the ‘non-ideal’ HC settings listed in Table 2. The blue curves correspond to the ‘ideal HC’ setting

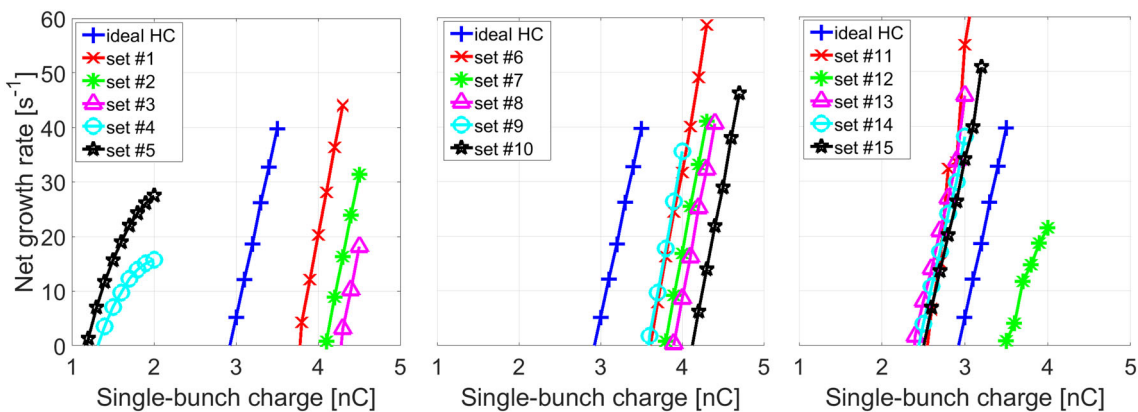


**Fig. 8** (Color online) Net TMCI growth rates for different single-bunch charges, corresponding to the ‘non-ideal’ HC settings listed in Table 2. The blue ‘+’ markers represent the ‘ideal HC’ setting

category. Analyses showed that some ‘non-ideal lengthening’ conditions can indeed be used to increase either the MWI or the TMCI threshold charges relative to ‘ideal lengthening’ conditions. More interestingly, some ‘non-

ideal lengthening’ conditions showed higher MWI and TMCI thresholds. Further analyses suggested that sub-ideal lengthening with more particles at the bunch tail increases

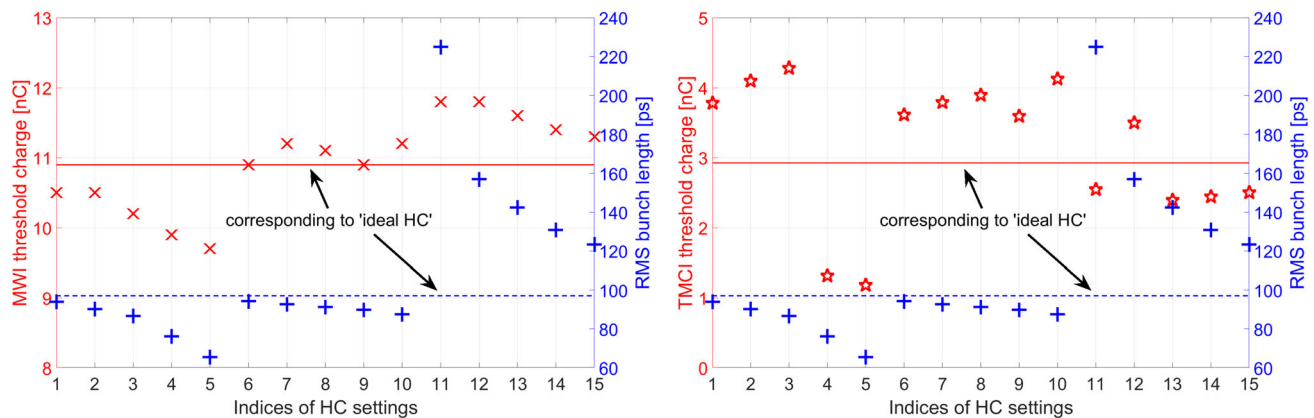


**Fig. 9** (Color online) Threshold charges for (left) MWI and (right) TMCI, vs. the indices of HC settings, together with the RMS bunch lengths. Left: the red cross markers represent the MWI threshold charges obtained using the aforementioned ‘1 % growth policy’. The red line indicates the MWI threshold charge under the ‘ideal HC’ setting. Right: the red pentagram markers represent the TMCI

threshold charges. The red line indicates the TMCI threshold charge corresponding to ‘ideal HC’. The blue + markers in both the left and the right plots represent the RMS bunch lengths corresponding to the different HC settings without considering any collective effect. The blue dashed line indicates the RMS bunch length under ‘ideal HC’ conditions

the probability of increasing MWI and TMCI threshold charges simultaneously.

Before discussing the underlying physical mechanism, we note that at least two conditions must be satisfied to produce a single-bunch instability: the driving wakefield must be sufficiently strong, and the number of particles experiencing this wakefield must be sufficiently large. Putting more particles at the bunch tail implies the existence of a stronger short-range wakefield near the bunch tail. Because of causality, most particles in a single bunch cannot sense a strong wakefield. This implies that putting more particles in the bunch tail reduces the number of particles in a single bunch that experience a strong wakefield.

We argue that this increase in MWI and TMCI thresholds can be explained qualitatively by considering that, with fewer electrons in the bunch head, the particles in the bunch head drive a weaker wakefield, regardless of whether it is longitudinal or transverse. Therefore, the motion of the trailing particles is less disturbed because they experience a weaker wake force. On the other hand, despite having more particles at the bunch tail driving a stronger wakefield behind, the influence on the single-bunch instabilities is less important because there are only a few trailing electrons behind the ‘bunch tail’.

However, this explanation remains phenomenological and no theory so far predicts the optimal HC setting for single-bunch instabilities. In the ongoing development of a more general theory, more systematic studies remain to be done on the influences of HCs on single-bunch instabilities in electron storage rings.

**Acknowledgements** Most simulations were performed on the cluster operated by the IHEP computing center. The authors appreciate the kind support provided by the staff at the IHEP computing center.

**Author Contributions** All authors contributed to the study conception and design. Material preparation, data collection and analysis were performed by Hai-Sheng Xu, Jing-Ye Xu and Na Wang. The first draft of the manuscript was written by Hai-Sheng Xu and all authors commented on previous versions of the manuscript. All authors read and approved the final manuscript.

## References

1. J.M. Byrd, M. Georgsson, Lifetime increase using passive harmonic cavities in synchrotron light sources. *Phys. Rev. ST Accel. Beams* **4**, 030701 (2001). <https://doi.org/10.1103/PhysRevSTAB.4.030701>
2. M. Georgsson, A. Andersson, M. Eriksson, Landau cavities at MAX-II. *Nucl. Instrum. Meth. Phys. Res. A* **416**, 465–474 (1998). [https://doi.org/10.1016/S0168-9002\(98\)00667-6](https://doi.org/10.1016/S0168-9002(98)00667-6)
3. M. Svandrlík, G. Penco, P. Craievich et al., Performance of the 3rd harmonic superconducting cavity at ELETTRA. In: *Proceedings of the 11th Workshop on RF Superconductivity, Lubeck/Travemunder, Germany* (2003)
4. M. Pedrozzi, J.-Y. Gloor, W. Gloor et al., SLS operational performance with third harmonic superconducting system. In: *Proceedings of the 11th Workshop on RF Superconductivity, Lubeck/Travemunder, Germany* (2003)
5. G.M. Ma, Z.T. Zhao, J.F. Liu, Design of a higher harmonic cavity for the SSRF storage ring. *Chin. Phys. C* **32**, 275 (2008). <https://doi.org/10.1088/1674-1137/32/4/007>
6. T. Phimsen, B.C. Jiang, H.T. Hou et al., Improving Touschek lifetime and synchrotron frequency spread by passive harmonic cavity in the storage ring of SSRF. *Nucl. Sci. Tech.* **28**, 108 (2017). <https://doi.org/10.1007/s41365-017-0259-y>
7. R. Nagaoka, K.L.F. Bane, Collective effects in a diffraction-limited storage ring. *J. Synchrotron Rad.* **21**, 937–960 (2014). <https://doi.org/10.1107/S1600577514015215>

8. P.F. Tavares, S.C. Leemann, M. Sjoström et al., The MAX IV storage ring project. *J. Synchrotron Rad.* **21**, 862–877 (2014). <https://doi.org/10.1107/S1600577514011503>
9. A. Streun, T. Garvey, L. Rivkin et al., SLS-2: the upgrade of the Swiss Light Source. *J. Synchrotron Rad.* **25**, 631–641 (2018). <https://doi.org/10.1107/S1600577518002722>
10. Y. Jiao, G. Xu, X.-H. Cui et al., The HEPS project. *J. Synchrotron Rad.* **25**, 1611–1618 (2018). <https://doi.org/10.1107/S1600577518012110>
11. C.G. Schroer, I. Agapov, W. Brefeld et al., PETRA IV: the ultralow-emittance source project at DESY. *J. Synchrotron Rad.* **25**, 1277–1290 (2018). <https://doi.org/10.1107/S1600577518008858>
12. S.C. Jiang, G. Xu, Examining RF jitter and transverse mode-coupling instability in triple-frequency RF systems. *Nucl. Sci. Tech.* **31**, 45 (2020). <https://doi.org/10.1007/s41365-020-00752-3>
13. H.S. Xu, N. Wang, Influences of harmonic cavities on the single-bunch instabilities in electron storage rings. In Proceedings of FLS2018, Shanghai, China (2018). <https://doi.org/10.18429/JACoW-FLS2018-WEP2PT024>
14. R. Hettel, DLSR design and plans: an international overview. *J. Synchrotron Rad.* **21**, 843–855 (2014). <https://doi.org/10.1107/S1600577514011515>
15. M. Venturini, Harmonic cavities and the transverse mode-coupling instability driven by a resistive wall. *Phys. Rev. Accel. Beams* **21**, 024402 (2018). <https://doi.org/10.1103/PhysRevAccelBeams.21.024402>
16. S.Y. Lee, *Accelerator Physics*, 4th edn. (World Scientific, Singapore, 2019)
17. M. Borland, Elegant: A flexible SDDS-compliant code for accelerator simulation. In: Advanced Photon Source LS-287, Argonne National Laboratory (2000)
18. Y. Wang, M. Borland, Pelegant: A parallel accelerator simulation code for electron generation and tracking. *AIP Conf. Proc.* **877**, 241 (2006). <https://doi.org/10.1063/1.2409141>
19. D. Boussard, Observation of microwave longitudinal instabilities in the CPS. Report LABII/RF/Int./75.2